Vortical flow control on a conical fore body cross section using an array of pulsed dc actuators

Kunwar Pal Singh and Subrata Roy[a)]
Computational Plasma Dynamics Laboratory and Test Facility,
Department of Mechanical and Aerospace Engineering, University of Florida, Gainesville, Florida 32611

(Received 22 November 2006; accepted 23 February 2007; published online 1 May 2007)

Flow control on a conical fore body cross section of an aircraft is studied using plasma discharge by considering the neutral gas flow at 17.5 deg angle of attack. The equations governing the motion of electrons, ions as well as Poisson's equation are solved together with Navier-Stokes and energy equation for neutrals to study flow control. A single barrier discharge actuator is not sufficient to control the flow on the entire length of the fore body. An arrangement of multiple electrodes powered with pulsed dc voltage has been suggested for controlling such flows. The effects of joule heating of plasma, dielectric heating, and electrodynamic force have been investigated, separately and then combined on flow control. It is found that joule heating results in high temperature of the dielectric surface, however; electrodynamic force contributes prominently to flow control. A three-dimensional analysis is necessary to validate results with experiments. © *2007 American Institute of Physics*. [DOI: 10.1063/1.2720256]

I. INTRODUCTION

Surface barrier discharges in asymmetric configurations have been proposed as actuators for flow control in aerodynamic applications. These actuators have proved effective for flow attachment in internal and external aerodynamics, and for modification of the lift, drag, and stall angle of airfoils. The electrical properties of an asymmetric surface dielectric barrier discharge in atmospheric air have been investigated experimentally.[1] Effects of different discharge parameters and their temporal force have been measured for a range of frequencies and voltages to determine the mechanism of transfer of momentum to the air by the plasma actuator.[2] Control parameters for separation mitigation using an asymmetric single dielectric barrier plasma actuator have been studied by current authors.[3] The results show the body force is proportional to frequency and increases with the increase in voltage. Both phenomenological and first-principles models have been employed to resolve the effect of the volume force in controlling three-dimensional laminar and transitional flow structures in a loosely coupled fluid plasma formulation.[4] Several applications including suppression of NACA 0015 wing stall, control of boundary layer transition on a flat plate, control of laminar separation over a ramp, and turbulent separation over a wall-mounted hump were investigated. For moderate Reynolds numbers either coflow or counter-flow pulsed actuators with sufficiently high frequency were found to be able to mitigate wing stall. Unsteady flow actuation with a duty cycle showed better results than continuous steady operation of the plasma actuator. Analysis of a backward hump flow demonstrated that once the flow is turbulent, the actuator strength needs to be beyond a threshold for effective flow control implying scalability of dielectric barrier discharge (DBD) devices to higher free-stream velocities for practical problems.

Instantaneous flow velocity induced by surface plasma actuators in air at atmospheric pressure has been measured.[5] Power transfer to the neutral gas flow by ion-neutral collisions has been improved by adjustment of the actuator geometry, materials, rf frequency and rms voltage.[6] Simultaneously, power losses due to inadequate impedance matching of the power supply to the actuator, dielectric heating, and power required to maintain the atmospheric pressure plasma have been reduced for better performance of actuator. Laminar airfoil design employing a separation ramp at the trailing edge that can be manipulated by a plasma actuator to control lift has been studied.[7] The experiments on a two-dimensional (2D) airfoil section mounted on a lift-drag force balance demonstrate lift enhancement produced by the plasma actuator comparable to a plane flap. This apparently has the advantage of reducing the actuator power by 90%.[7]

Flight vehicle fore-body vortex symmetry breaking and control of resulting yaw departure by surface plasma discharges have been studied analytically for a circular cone.[8] The authors analyzed stability of the point vortices to small symmetric and asymmetric displacements and validated analytical results against experimental results. Surface discharge plasmas to control or eliminate vortical asymmetry about the nose of a conical fore body at an angle of incidence have been studied, using high-frequency spark discharge plasma to control vortex positions on the conical fore body.[9] Results

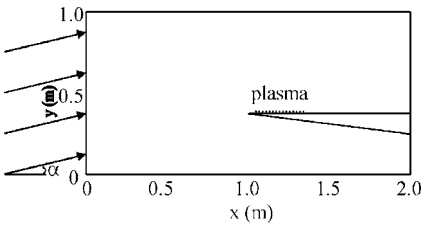

FIG. 1. Schematic of flow control on a fore body of an aircraft using plasma discharge with an incident gas flow at angle α.

[a)]Electronic address: roy@ufl.edu

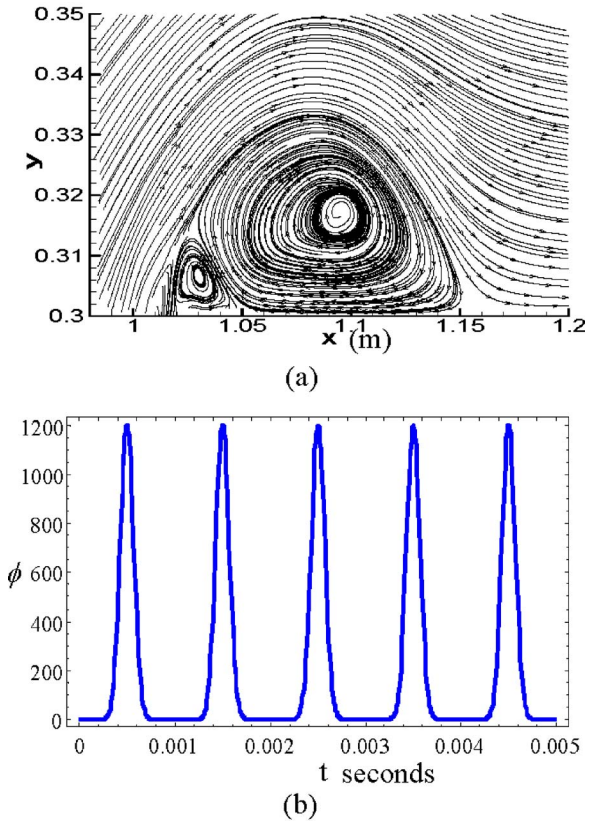

FIG. 2. (a) Streamlines and vectors of gas velocity at the end of 0.1 s without any discharge, and (b) temporal profile of pulse dc voltage.

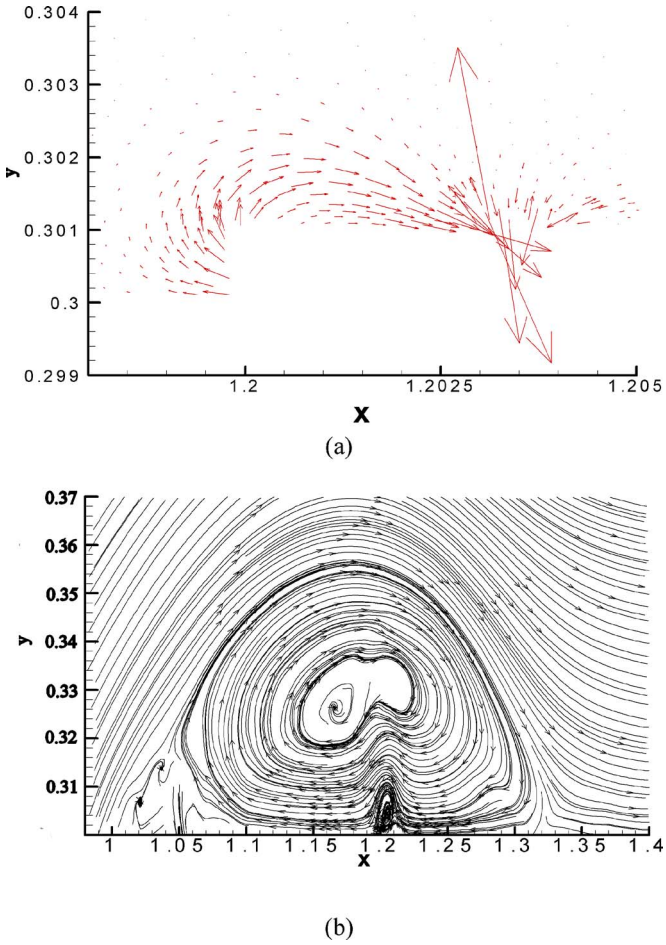

FIG. 3. (a) Streamlines and vectors of gas velocity after 50 cycles of dielectric barrier discharge, and (b) time averaged electrodynamic force vectors due to dielectric barrier discharge. x and y are in meters.

of wind tunnel experiments show that plasma discharges distributed in the model nose region near flow separation lines may be used for successful control or elimination of vortex asymmetry.

In this article, we study flow control on the fore body of an aircraft using plasma discharge by considering the neutral gas flow at an angle of attack. The physics of a surface barrier discharge operated with a neutral gas has been investigated by many researchers.[10] A sinusoidal or pulsed excitation signal has been applied and the temporal and spatial profiles of excited species and its interaction with neutrals have been determined.

Here, a single DBD actuator and an arrangement of pulsed dc voltage plasma discharge have been investigated to control the flow. The effects of joule heating of plasma, dielectric heating, and electrodynamic force have been investigated separately and then combined on flow control. Geometry description is given in Sec. II, governing equations in Sec. III, initial and boundary conditions are given in Sec. IV, results and discussion in Sec. V, and conclusion are drawn in Sec. VI.

II. GEOMETRY DESCRIPTION

Schematic of flow control on the fore body of an aircraft using plasma discharge with an incident gas flow angle α is shown in Fig. 1. The width of the domain is 2 m and the height is 1 m. The gas is incident at an angle $\alpha=15°$ (17.5° with the centerline of the fore body) with 10 m/s velocity. The angle at the nose of the fore body is 5°. We have studied two electrode configurations for this fore-body geometry, one with dielectric barrier discharge plasma actuator and another with seven pairs of electrodes powered with pulsed dc voltage. The thickness of electrodes is assumed infinitesimally small for both cases. Following is the description of the configuration with dielectric barrier discharge plasma actuator. The dielectric is located between $x=1.2$ m and $x=1.21$ m with dielectric thickness equal to 1.0 mm. The rf electrode is exposed and is located at $x=1.203$ m to $x=1.204$ m at $y=0.301$ m. Grounded electrode is $x=1.206$ m to $x=1.207$ m at $y=0.3$ m. The electrodes for pulsed dc configuration are located at $y=0.3$ m, and from $x=1.05$ to 1.172 m. Length of each electrode is 2 mm and the distance between electrodes is 8 mm. There are seven pairs of electrodes. Each pair is powered by a pulsed dc potential specified below.

III. GOVERNING EQUATIONS

The drift-diffusion form of continuity and Poisson's equations for the electrons and ions are solved together with the following fluid momentum and continuity equations:

$$\frac{\partial n_\alpha}{\partial t} + \nabla(n_\alpha \mathbf{v}_\alpha) = n_e S$$

$$\text{with } n_\alpha \mathbf{v}_\alpha = -\operatorname{sgn}(e) n_\alpha \mu_\alpha \nabla \phi - D_\alpha \nabla n_\alpha$$

$$\text{for } \alpha = e, i, \tag{1a}$$

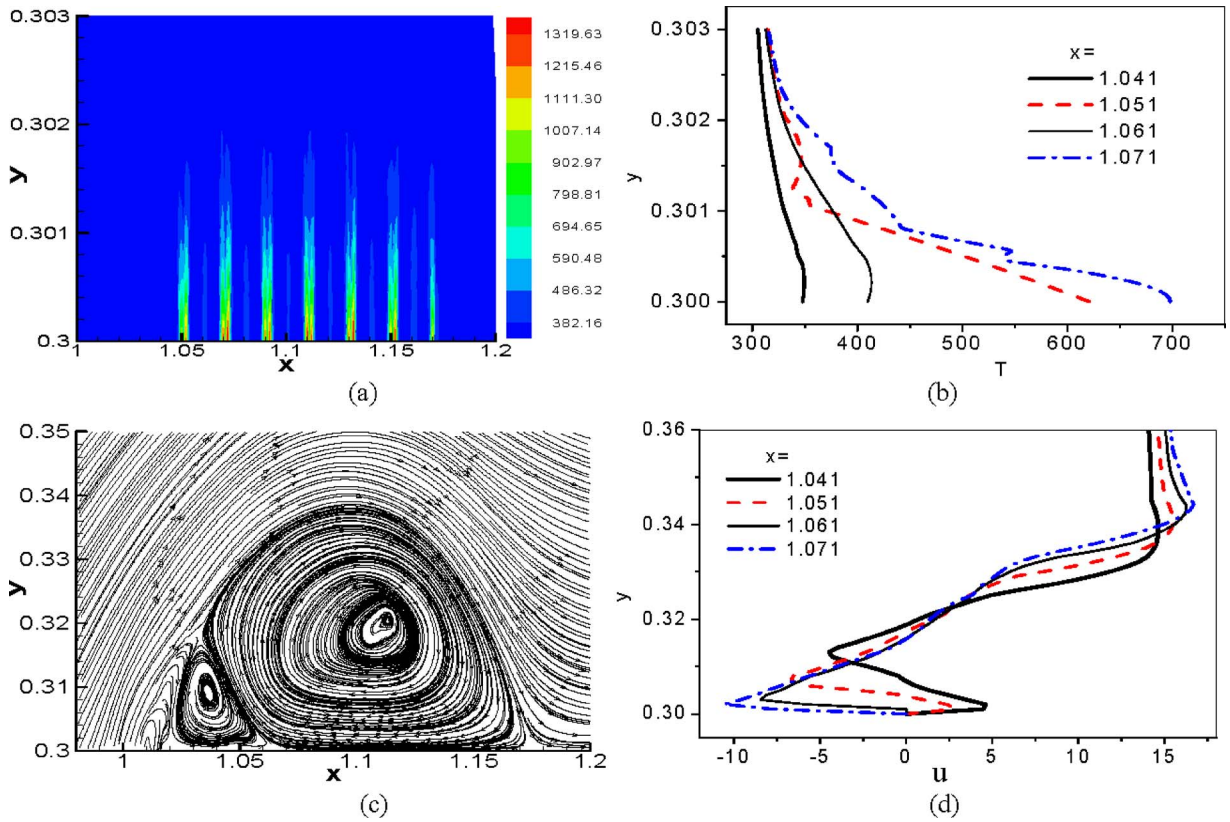

FIG. 4. (a) Gas temperature due to joule heating, (b) gas temperature (in kelvin) as a function of y (in meters), (c) streamlines and vectors of gas velocity, and (d) gas velocity components u (in meters/seconds) as a function of y (in meters).

$$\varepsilon \nabla^2 \phi = e(n_e - n_i), \tag{1b}$$

$$\rho \frac{\partial \mathbf{u}}{\partial t} - \nabla(\eta \nabla \mathbf{u}) + \rho(\mathbf{u} \cdot \nabla)\mathbf{u} + \nabla p = e(n_e - n_i) \nabla \phi, \tag{2a}$$

$$\frac{\partial \rho}{\partial t} + \nabla(\rho \mathbf{u}) = 0, \tag{2b}$$

$$\rho C_p \frac{\partial T}{\partial t} + \nabla(k \nabla T + \rho C_p T \mathbf{u}) = \mathbf{J} \cdot \mathbf{E} + \frac{1}{2} \frac{\partial}{\partial t}(\varepsilon_0 \varepsilon_r \mathbf{E})\mathbf{E}, \tag{3}$$

where n_e, n_i, ρ, $\mathbf{v}_e$, $\mathbf{v}_i$, and $\mathbf{u}$ are densities and velocities of electrons, ions, and the working gas, respectively. η is the gas viscosity, S is the Townsend ionization rate, pressure $p = \rho RT/M$, M (mole/gm) is the molar mass of helium, T is the temperature (300 K), and R is the universal gas constant [erg/(mole K)]. $\mathbf{J}$ is total (electron and ion) current density and $\mathbf{E}$ is the electric field. The bulk density of the helium is taken to be 1.79×10^{-4} g/cm^3, and the viscosity is assumed to be 1.9 poise. First and second terms of Eq. (3) on the right-hand side represent joule and dielectric heating, respectively.

IV. INITIAL CONDITIONS AND BOUNDARY CONDITIONS

Initial electron and ion densities are 10^9 m^3. Initial voltage is zero, initial u and v velocities are 9.65 and 2.58 m/s, respectively. Initial air density is 1.2 Kg/m^3 and initial gas temperature is 300 K.

Boundary conditions for Poisson's equation are set as follows: potential $\phi = \phi_0 \sin(50\,000\pi t)$ for the DBD case, with $\phi_0 = 500$ V and $\phi = \phi_0 \sin^{20}(1000\pi t)$. For pulsed dc voltage case $\phi_0 = 1200$ V. The potential is applied to the first electrode of the pair for pulsed dc case. Other electrodes of each pair are grounded. Electric insulation condition (normal component of electric field equal to zero) is assumed at outer boundaries of the domain and at the surface of the fore body.

The following are boundary conditions related to electrons and ions continuity equations: The currents flow normal only to the electrodes, since these are equipotential surfaces. Homogeneous Neumann conditions are applied to the outer edges of the domain and electric insulation is assumed at the surface of the fore body and dielectric. The currents flow normal as well as parallel to the dielectric surface.

The boundary conditions for Navier-Stokes equations are as follows: The no-slip condition ($u = 0$ and $v = 0$) is assumed for the gas neutrals at the surface of fore-body, dielectric surface (for dielectric barrier discharge case) and at electrodes. The velocity at the left boundary of the upper domain is set equal to the initial condition ($u = 9.65$ m/s and $v = 2.58$ m/s). Neutral boundary conditions are applied to the outer edges of the domain.

The self-consistent formulation is solved using a Galerkin variational formulation based finite-element method to obtain electron and ion density, electric potential, neutral velocity, density, and gas temperature.

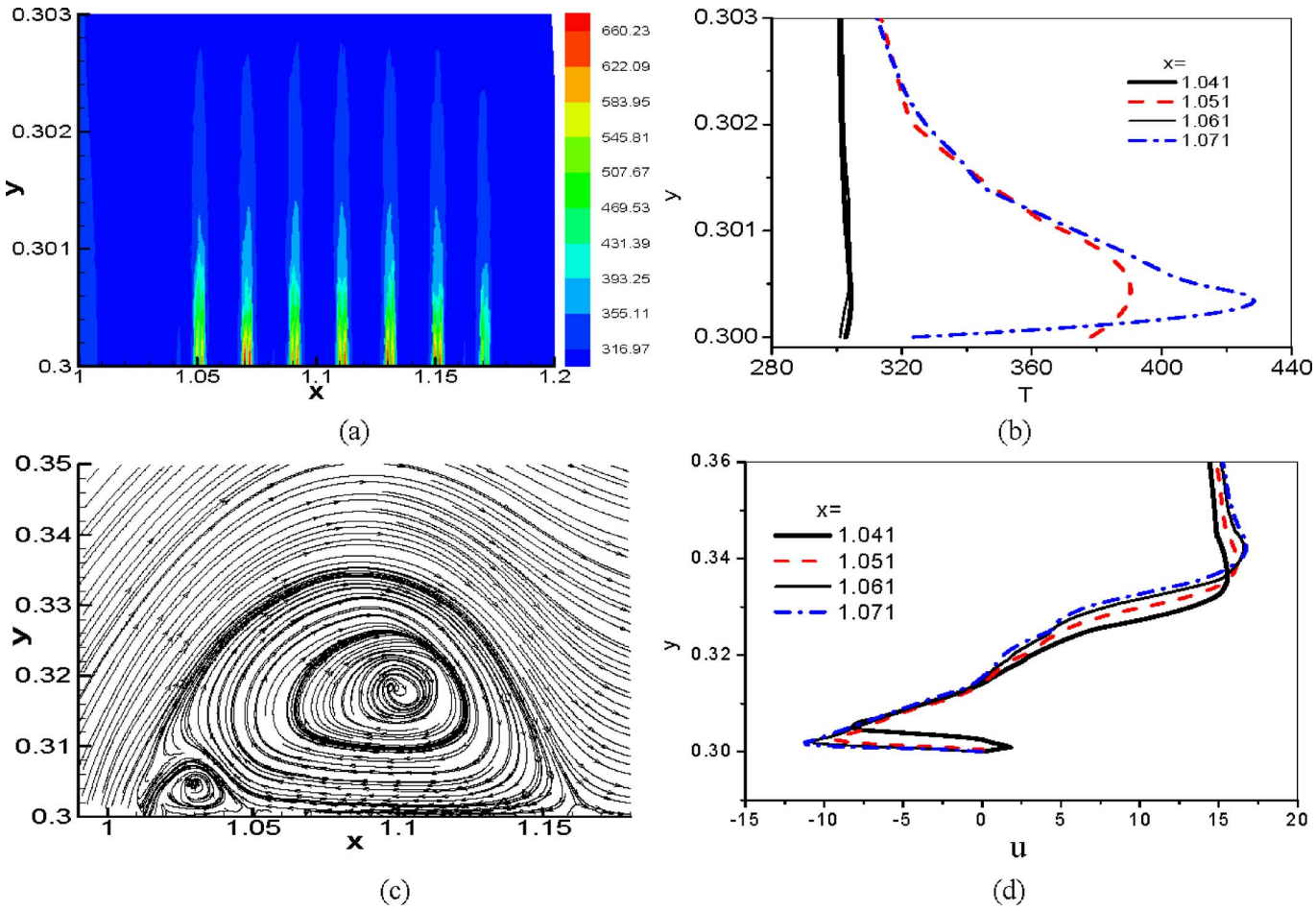

FIG. 5. (a) Gas temperature due to dielectric heating, (b) gas temperature (in kelvin) as a function of y (in meters), (c) streamlines and vectors of gas velocity, and (d) gas velocity components u (in meters/seconds) as a function of y (in meters).

V. RESULTS AND DISCUSSION

We describe our fluid dynamic simulation results in the following paragraphs. Figure 2(a) shows streamlines and vectors of gas velocity at the end of 0.1 s without any plasma discharge, obtained by solving Navier-Stokes equations. We can see a recirculation bubble near the nose of the fore body. These kinds of separation bubbles are harmful to the performance of the aircraft. A rf voltage (for DBD) or a pulsed dc voltage is switched on after 0.1 s to see the effect. Figure 2(b) shows the profile of pulsed dc voltage as a function of time. Figure 3 displays results for dielectric barrier discharge after 25 cycles of plasma discharge activity, and Figs. 4–7 show results for pulsed dc plasma discharge after 10 cycles of plasma discharge activity.

Figure 3 shows the effect of dielectric barrier discharge plasma actuator on flow control on the fore body of an aircraft. We do not solve temperature Eq. (3) for the results shown in this figure. After 0.1 s rf voltage $\phi=\phi_0 \sin(2\pi f)$; with $\phi_0=500$ V and $f=25$ kHz, is switched on to see the effect. Figure 3(a) shows vectors of time averaged electrodynamic force $e(n_i-n_e)\mathbf{E}$. It can be seen from the figure that force is directed in forward direction which may help in elimination of recirculation. Figure 3(b) shows streamlines and vectors of gas velocity after 25 cycles of rf discharge activity. We can see that recirculation is affected by a dielectric barrier discharge plasma actuator, however, flow is not attached to the surface all over the surface of the fore body. This is because a single dielectric barrier plasma actuator is not sufficient to cover the entire length of recirculation and recirculation is not eliminated fully. Multiple dielectric barrier discharge plasma actuators on the surface of the fore body may control vortex dynamics of the flow. We suggest multiple pairs of electrodes powered with pulsed dc potential as an alternative to multiple DBD plasma actuators in this paper.

We have included joule heating effect in Navier-Stokes equations for the results of Fig. 4. We have added Eq. (3) to the set of equations described under governing equations and have only considered the joule heating term. The force term in the Navier-Stokes equation is set to zero as we want to know effect of joule heating of plasma alone on the flow control. Figure 4(a) shows distribution of temperature. Maximum temperature is near the dielectric surface or electrodes because total current is highest here due to high-electric field. The temperature rises up to nearly 1400 K, which means there is a significant rise in temperature above normal temperature of 300 K due to joule heating. Figure 4(b) shows gas temperature (in kelvin) as a function of y for different values of x. Figure 4(c) shows streamlines and vectors of gas velocity after ten cycles of plasma discharge activity by a

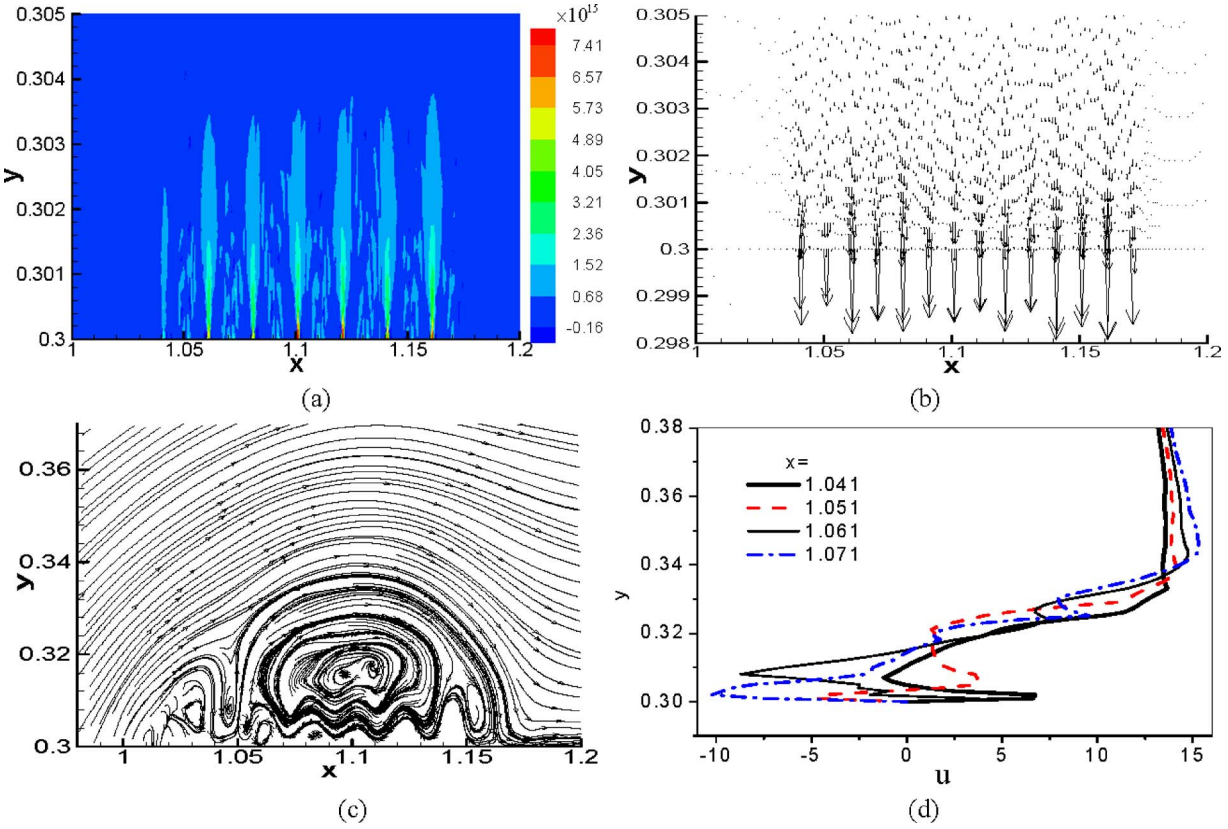

FIG. 6. (a) Charge separation $(n_i - n_e)$ distribution at the peak of the pulsed dc, (b) time averaged electrodynamic force vectors, (c) streamlines and vectors of gas velocity, and (d) gas velocity components u (in meters/seconds) as a function of y (in meters).

pulsed dc voltage. If we compare Figs. 2(a) and 4(c) we can see that there is negligible change in flow pattern after ten cycles of plasma discharge activity. Recirculation is affected very little by joule heating of a pulsed dc voltage and flow is not attached to the surface. Figure 4(d) shows gas velocity components u (in meters/second) as a function of y (in meters) for different values of x as a result of joule heating effect.

We have included dielectric heating effect in Navier-Stokes equations for the results of Fig. 5 by taking into account dielectric heating only in Eq. (3). The force term in the Navier-Stokes equation is set to zero, so as to investigate the dielectric heating effect alone on flow control. Displacement current through the dielectric results in high temperatures on the dielectric surface. Figure 5(a) shows temperature distribution in the domain. The temperature rises up to nearly 675 K, which is higher than the normal temperature of 300 K. The rise in temperature of the gas is confined very close to dielectric surface only. Figure 5(b) shows gas temperature (in kelvin) as a function of y. Figure 5(c) shows streamlines and vectors of gas velocity after ten cycles of plasma discharge activity by a pulsed dc voltage. If we compare Figs. 2(a) and 5(c), we can see that there is only a small change in the flow pattern due to dielectric heating after ten cycles of plasma discharge activity. It means that the role played by dielectric heating due to pulsed dc voltage in not a major consideration in flow control. Figure 5(d) shows gas velocity components u (in meters/second) as a function of y (in meters) as a result of dielectric heating.

Figure 6 shows the effect of plasma discharge upon flow control on the fore body of an aircraft due to electrodynamic force only. Hence, the electrodynamic force term has been included in Navier-Stokes equations and temperature Eq. (3) has been excluded. Figure 6(a) shows charge separation and vectors of electrodynamic force at the peak of the spike. Figure 6(b) shows vectors of time averaged electrodynamic force $e(n_i - n_e)\mathbf{E}$. It can be seen from the figure that force is directed mostly downward which helps in destruction of the big recirculation bubble and results in formation of small bubbles. Figure 6(c) shows streamlines and vectors of gas velocity after ten cycles of plasma discharge activity by a pulsed dc potential. We can see that the effect of plasma discharge on recirculation is the highest in this case. A big recirculation bubble is destroyed and small bubbles are formed which may not be as harmful to the performance of the aircraft. Figure 6(d) shows gas velocity components u (in meters/second) as a function of y (in meters) due to electrodynamic force.

We also want to see the combined effect played by different factors on flow control on a fore body. Effects due to joule heating, dielectric heating, and electrodynamic force have been combined in the results of Fig. 7. The electrodynamic force term in Navier-Stokes equations and joule heating and dielectric heating terms in temperature Eq. (3) have been retained. Figure 7(a) shows temperature distribution. The temperature rises up to 1605 K, which is slightly higher than joule heating alone in Fig. 4 due to a combined effect. Figure 7(b) shows gas temperature (in kelvin) as a function

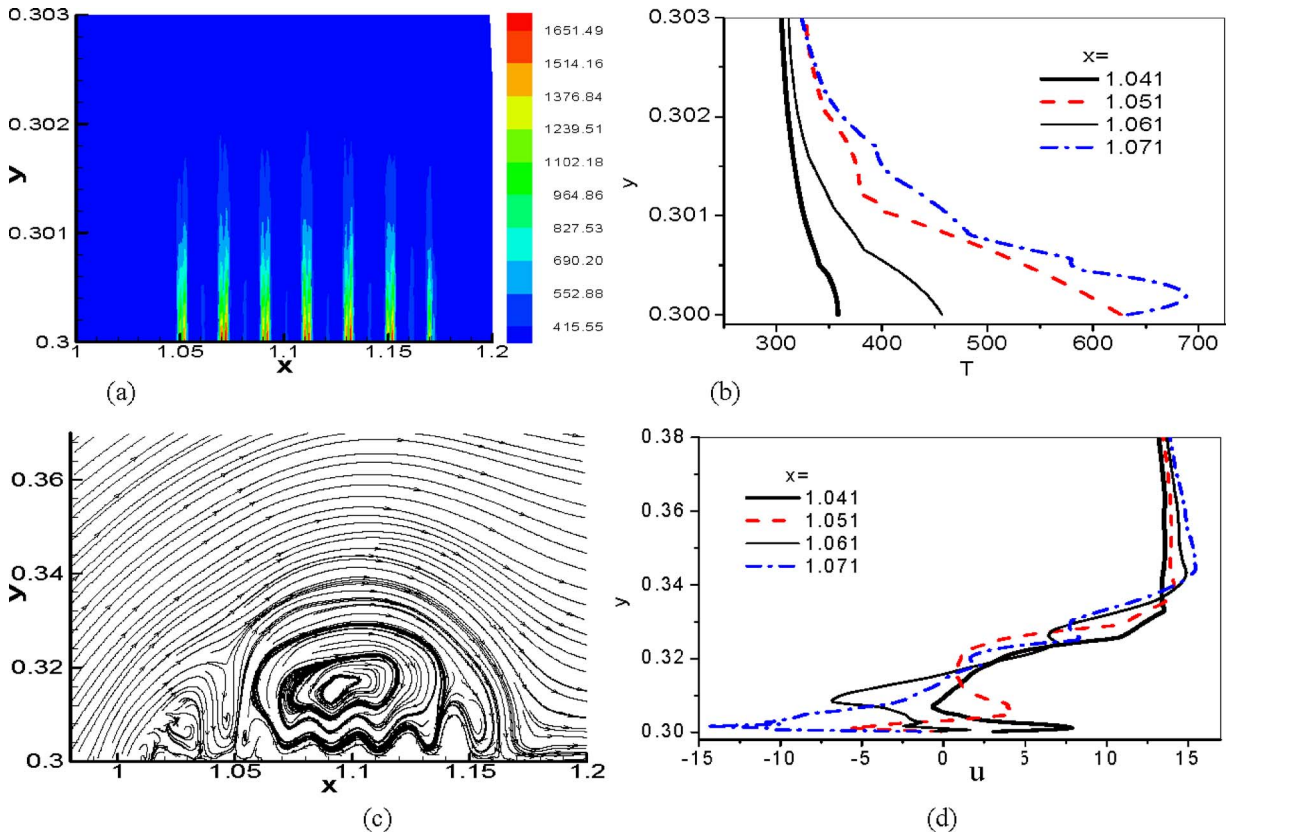

FIG. 7. (a) Gas temperature due to combined effects of dielectric and joule heating, and (b) gas temperature (in kelvin) as a function of y (in meters), (c) streamlines and vectors of gas velocity, and (d) gas velocity components u (in meters/seconds) as a function of y (in meters) as a result of combined dielectric heating, joule heating, and electrodynamic force.

of y at different values of x. Figure 7(c) shows streamlines and gas velocities. Figure 7(d) shows gas velocity components u (in meters/second) as a function of y (in meters) at different values of x as a result of combined dielectric heating, joule heating, and electrodynamic force. If we compare Figs. 6(c) and 7(c), we can see that there is not much difference between the two figures. We can conclude that effect played by electrodynamic force is highest on flow pattern.

In the following paragraphs we calculate power density analytically. One-dimensional analysis has been used for simplicity. We have not considered dielectric heating in the following analysis as we found in our numerical simulations that power density due to dielectric heating is small as compared to the joule heating.

A. Power density due to joule heating

$$P_J = \mathbf{J} \cdot \mathbf{E} = (-en_e\mathbf{v}_e + en_i\mathbf{v}_i)\mathbf{E}.$$

Electron current will dominate due to high mobility of electrons. The x component of the electric field is much higher than the y-component.

$$P_J \approx e(n_e\mu_e + n_i\mu_i)E_x^2.$$

Average value of power density due to joule heating can be found as follows:

$$P_{J\,\text{average}} \approx e(n_e\mu_e + n_i\mu_i)E_0^2\frac{1}{T}\int_0^T \sin^{40}(2\pi ft)dt,$$

$$P_{J\,\text{average}} \approx 0.125e(n_e\mu_e + n_i\mu_i)E_0^2. \quad (4)$$

B. Power density due to electrodynamic force

$$P_E = \mathbf{F}_q \cdot \mathbf{v}_q = e(n_i - n_e)\mathbf{E} \cdot \mathbf{v}_q,$$

$$P_E \approx e(n_i - n_e)\mathbf{v}_q E_x \approx e(n_i - n_e)\mu_i E_0^2 \sin^{40}(2\pi ft).$$

Average value of power density due to electrodynamic force can be found as follows:

$$P_{E\,\text{average}} \approx e(n_i - n_e)\mu_i E_0^2\frac{1}{T}\int_0^T \sin^{40}(2\pi ft),$$

$$P_{E\,\text{average}} \approx 0.125e(n_i - n_e)\mu_i E_0^2. \quad (5)$$

C. Ratio between the two power densities

$$\frac{P_E}{P_J} \approx \frac{(n_i - n_e)\mu_i}{(n_i\mu_i + n_e\mu_e)}. \quad (6)$$

For $\mu_i = 2.4 \times 10^{-3}$ and $\mu_e = 0.176$ (both in SI units), Eq. (6) becomes

$$\frac{P_E}{P_J} \approx \frac{0.0136(n_i/n_e - 1)}{(0.0136n_i/n_e + 1)}. \quad (7)$$

If $n_i \gg n_e$ then

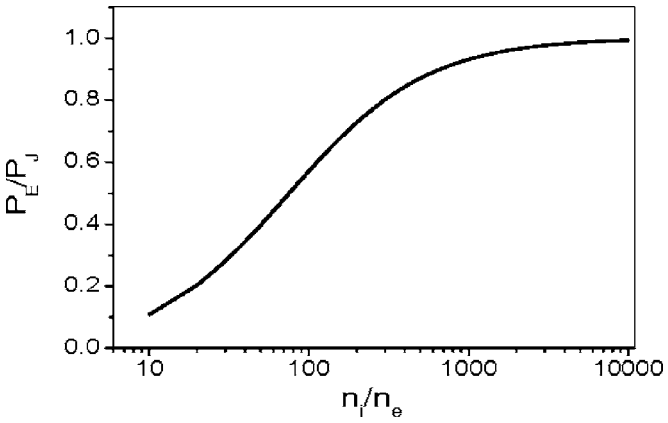

FIG. 8. Variation of P_E/P_J as a function of n_i/n_e. The parameters are same as in Eq. (7).

$$\frac{P_E}{P_J} \approx 1.$$

This implies that the power densities due to electrodynamic force and due to joule heating are nearly the same for $n_i \gg n_e$. Near the surface of the fore body n_i is much greater than n_e in our numerical simulations. Figure 8 shows variation of P_E/P_J as a function of ratio of ion density to electron density n_i/n_e. Even though power densities due to electrodynamic force and that due to joule heating are nearly the same, the effect of the former is dominant at low powers due to its strong coupling to the flow while joule heating affects flow through thermal boundary layer.

By adjusting the shape of the dc signal and the relative phases between potential applied to electrodes, we can further improve performance of flow control on a fore body. Plasma equations and Poisson's equation require more refined mesh than that for Navier-Stokes and temperature equations. Time scales of the equations are also different. This creates a problem of having a converging solution for all the equations together. Finding a time average of the force and current from plasma equations and then finding a space dependent function for force and current could yield faster though not as accurate solution of this pulsed dc actuation problem.

VI. CONCLUSIONS

Flow control on a fore body of an aircraft using plasma discharge is studied by considering the neutral gas flow at an angle of attack. Dielectric barrier discharge and pulsed dc plasma discharge have been used for flow control. The equations governing the motion of electrons, ions and Poisson's equation are solved with Navier-Stokes and temperature equation for neutrals to study flow control. A single DBD actuator affected flow over a limited region and was not sufficient to control the flow on the entire length of the fore body. An arrangement of multiple electrodes is suitable for elimination and/or control of vertical structures along the length of the fore body. We demonstrated such capability with a set of seven actuators powered with pulsed dc voltage. The effect of joule heating of plasma, dielectric heating, and electrodynamic force has been investigated separately on flow control to identify relative importance of the effects. It is found that joule heating results in high plasma temperature, however, it is the electrodynamic force that contributes prominently to flow control. The large separation bubble is broken into smaller eddies that may not be as destructive to the performance of aircraft. As a next step, it is imperative that a (loosely or fully coupled) three-dimensional analysis[4] is validated with the experimental data for vortical flow control.

ACKNOWLEDGMENTS

This work was partially supported by the AFOSR Grant No. FA9550-05–1-0074 monitored by John Schmisseur and the Air Force Research Laboratory Contract No. F33615-98-D-3210. The authors acknowledge receiving geometric details from Andrey Sidorenko and many thoughtful discussions with Norman Malmuth.

[1] J. Pons, E. Noreau, and G. Touchard, J. Phys. D **38**, 3635 (2005).
[2] C. O. Porter, J. W. Baughn, T. E. McLaughlin, C. L. Enloe, and G. I. Font, 44th AIAA Aerospace Sciences Meeting and Exhibit, January, Reno, Nevada, AIAA-2006-104 (AIAA, Washington, D.C., 2006).
[3] K. P. Singh, S. Roy, and D. V. Gaitonde, Plasma Sources Sci. Technol. **15**, 735 (2006).
[4] D. Gaitonde, M. Visbal, and S. Roy, 44th Aerospace Sciences Meeting, January, Reno, Nevada, AIAA-2006-1205 (AIAA, Washington, D.C., 2006); M. Visbal, D. V. Gaitonde, and S. Roy, 3rd AIAA Flow Control Conference, June, San Francisco, AIAA-2006-3230 (AIAA, Washington, D.C., 2006).
[5] M. Forte, L. Leger, J. Pons, E. Moreau, and G. Touchard, J. Electrost. **63**, 929 (2005).
[6] J. R. Roth and X. Dai, 44th AIAA Aerospace Sciences Meeting and Exhibit, January 9–12, Reno, Nevada, AIAA-2006-2103 (AIAA, Washington, D.C., 2006).
[7] T. C. Corke, B. Mertz, and M. P. Patel, 44th AIAA Aerospace Sciences Meeting and Exhibit, January 9–12, Reno, Nevada, AIAA-2006-1208 (AIAA, Washington, D.C., 2006).
[8] V. Shalaev, A. Fedorov, N. Malmuth, V. Zharov, and I. Shalaev, 41st Aerospace Sciences Meeting and Exhibit, January 6–9, Reno, Nevada, AIAA-2003-34 (AIAA, Washington, D.C., 2006).
[9] A. A. Maslov, B. Y. Zanin, A. A. Sidorenko, B. V. Postnikov, V. P. Fomichev, A. D. Budovsky, and N. Malmuth, 43rd AIAA Aerospace Sciences Meeting and Exhibit 2005, Reno, Nevada, AIAA-2005–400 (AIAA, Washington, D.C., 2006).
[10] S. Roy, Appl. Phys. Lett. **86**, 101502 (2005); S. Roy and K. P. Singh, *ibid.* **89**, 011501 (2006); D. Korzec, E. G. Finantu-Dinu, M. Teschke, J. Engemann, M. Miclea, K. Kunze, J. Franzke, and K. Niemax, Plasma Sources Sci. Technol. **15**, 345 (2006).